International Journal of Pharmaceutics 386 (2010) 131–137

Contents lists available at ScienceDirect

International Journal of Pharmaceutics

journal homepage: www.elsevier.com/locate/ijpharm

A new sol–gel silica nanovehicle preparation for photodynamic therapy *in vitro*

Lin Zhou[a,b], Ji-Hua Liu[b], Jian Zhang[b], Shao-Hua Wei[a], Yu-Ying Feng[a], Jia-Hong Zhou[a,*], Bo-Yang Yu[b,**], Jian Shen[a]

[a] Jiangsu Key Laboratory Biofunctional Materials, Nanjing Normal University, Nanjing 210097, China
[b] Department of Complex Prescription of TCM, China Pharmaceutical University, Nanjing 211198, China

ARTICLE INFO

Article history:
Received 23 September 2009
Received in revised form 27 October 2009
Accepted 8 November 2009
Available online 14 November 2009

Keywords:
Silica nanovehicle
Hypocrellin A
Photodynamic therapy
Drug delivery system

ABSTRACT

We report a facile silica nanovehicle preparation procedure for hydrophobic drug delivery, which is carried out in water without adding any surfactant and additional catalyst. This strategy includes hydrophobic drug nanopaticle preparation by reprecipitation method and in situ hydrolyzation and polymerization to encapsulate this naoparticle using only *N*-(β-amimoethyl)-γ-aminopropyltyiethoxysilane (AETPS). To demonstrate this technique hypocrellin A (HA), a hydrophobic photosensitizing anticancer drug, is embedded into silica nanovehicle using this simple method. The resulting HA encapsulated nanovehicles (HANV) are monodisperse and stable in aqueous solution. Comparative studies with free HA and entrapped HA have demonstrated that the encapsulation effect on the embedded photosensitizer nanoparticle significantly enhances the efficacy of singlet oxygen generation and, thereby, the *in vitro* photodynamic efficacy.

1. Introduction

Photodynamic therapy (PDT) is considered as an innovative and attractive modality to treat localized and superficial tumors. After parental administration and preferential accumulation of photosensitizers (PSs) in malignant tissues, the therapeutic effect is triggered by light irradiation, through which the photon energy absorbed by PS is transferred to the environmental to generate reactive oxygen species (ROSs), such as singlet oxygen ($^1O_2$), resulting in death of the irradiated cell (Kim et al., 2009; Piao et al., 2008; Sadzuka et al., 2007). However, most photosensitizing drugs are hydrophobic and therefore, preparation of pharmaceutical formulations for parenteral administration is highly hampered. To overcome this difficulty, delivery vehicles have evolved to enable a stable dispersion of these drugs into aqueous systems. And there is substantial and growing interest in the development of silica nanovehicles for use in PSs delivery system that span both fundamental and applied research (Tang et al., 2005; Yan and Kopelman, 2003; Zhou et al., 2008; Zhou et al., 2009a,b).

Silica nanovehicles are especially suited for photodynamic therapy (PDT) since they will never release PS but allow active oxygen species (ROSs) such as $^1O_2$ to diffuse out through the micro-holes within the shell part of silica nanovehicles, that reduce the risk of toxicity and vascular clogging caused by free PSs aggregate into clusters in blood (Wang et al., 2004). The traditional methods to prepare silica nanovehicles are microemulsion/reverse microemulsion and stober sol–gel method (Piao et al., 2008). Microemulsion/reverse microemulsion method can effectively encapsulate PSs inside silica nanovehicles since this method provides a 'nano-reaction pool' (Kim et al., 2007; Roy et al., 2003). But the preparation procedures are complicated and in some cases, the residual surfactants or byproducts produced during the nanovehicles preparation tend to increase the systemic toxicity of the formulation. In contrast, there are no surfactants and little byproducts in stober sol–gel method. But most of the reaction system of sol–gel method is ethanol or methanol, so the prepared silica nanovehicle must be separated and re-dissolved in water. In recent years, the alcohol-free sol–gel route using tetramethyl orthosilicate (TMOS) to prepare silica composites was reported, but the results were not proper to PSs delivery system because some of the achievement were gels rather than of single particles and the others' water-solubility were poor (Corr et al., 2008; Ferrer et al., 2003; Frenkel-Mullerad and Avnir, 2005). Besides, the preparation process must be catalyzed by HCl and the PSs encapsulation efficacy is not satisfied since this method cannot provide the 'nano-reaction pool' and the unencapsulated PSs will absorb on the outside surface of these nanovehicles. To improve the encapsulation efficacy, PSs molecule was covalently linked with silane through chemical reaction, instead of just being physically encapsulated (Cheng et al., 2009; Hulchanskyy et al., 2007; Tu et al., 2009). Upon systemic administration, such method can greatly improve the encapsulation efficacy but this strategy increased the preparation

* Corresponding author. Tel.: +86 25 83598359; fax: +86 25 83598359.
** Corresponding author. Tel.: +86 25 83271383; fax: +86 25 85391042.
E-mail addresses: zhoujiahong@njnu.edu.cn (J.-H. Zhou), boyangyu59@163.com (B.-Y. Yu).

0378-5173/$ – see front matter © 2009 Elsevier B.V. All rights reserved.
doi:10.1016/j.ijpharm.2009.11.010

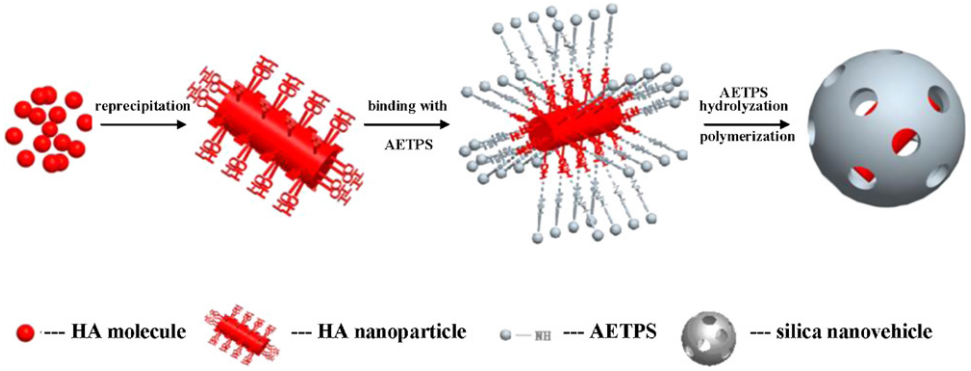

Scheme 1. Synthetic procedure of hypocrellin A nanoparticle encapsulated silica nanovehicle (HANV).

difficulty and limited its practical application. Therefore, there is an increasing interest to develop facile silica nanovehicle preparation methods which can effectively encapsulated PSs without adding any external agents such as surfactant or catalyst.

On the basis of these considerations, we reported a simple silica nanovehicles preparation procedure in water without adding surfactant and additional catalyst. This strategy included PSs nanopaticle preparation by reprecipitation method and in situ hydrolyzation and polymerization to encapsulate this naoparticle using *N*-(β-amimoethyl)-γ-aminopropyltyiethoxysilane (AETPS). Reprecipitation method is proposed as a good way to disperse hydrophobic compound in water. Hydrophobic compound was dissolved in organic solvent to prepare the stock solution. Then, mixing of the stock solution with the water phase rapidly changes the character of the solvent and induces nucleation and self-assemble as pure nanosized particles. The result PSs nanoparticles can remain stably dispersed in water for a long time (An et al., 2002; Baba et al., 2007; Fu and Yao, 2001; Xiao et al., 2003; Zhou et al., 2009a,b). We chose only AETPS to encapsulate PSs nanoparticles because the hydrolyzation speed of AETPS is slow enough to control and the hydrolysate can polymerize catalysed by its own alkalescence. This method is very facile but the encapsulation efficacy is satisfied.

As a proof of this concept, we have synthesized silica nanovehicles embedded hypocrellin A nanoparticles and the procedure for the preparation of HANV is illustrated in Scheme 1. First, HA nanoparticle was prepared by "reprecipitation method". Second, HA nanoparticle was surrounded by AETPS molecules through intermolecular hydrogen bonding between the hydroxyl groups of HA and the amine moieties of AETPS. Third, AETPS molecules were hydrolyzed and polymerized in situ to encapsulate the HA nanoparticle. Comparing with free HA, the embedded HA shows superior light-stability and singlet oxygen generation ability. Also presented is experiment showing the enhanced efficacy *in vitro* PDT, to demonstrate the validity and potential for using it as drug carrier in PDT.

2. Materials and methods

2.1. Chemicals

N-(β-aminoethyl)-γ-aminopropyl-triethoxysilane (AEAPS), tetramethylorthosilicate (TMOS) and 9,10-anthracenedipropionic-acid were purchased from Sigma; Rhodamine-123, DiOC6 (3), bodipy and lucifer yellow from Molecular Probe; Hoechest 33342 from Amosco; 2′7′-Dichlorofluorescin diacetate (DCFH-DA) kit from Beyotime; Dulbecco's minimum essential medium (DMEM) from Gibico and 3-[4,5-dimethylthiazol-2-yl]-2,5-diphenyl tetrazoliumbromide (MTT) from Amosco.

2.2. Preparation and characterization of drug-loaded silica nanovehicles

In a typical experiment, 20 mL 60 μM HA nanoparticles aqueous solution was prepared as protocol method (Zhou et al., 2009a,b). Then, 0.2 mL AEPTS was added to above solution and the mixed solution was stirred vigorously at room temperature for 24 h before the reaction was stopped. Finally, the byproduct in the solution was removed by dialysis against water with a 12–14 kDa molecular weight cut off cellulose membrane for 12 h. Transmission electron microscopy (TEM) was employed to determine the morphology and size of the aqueous dispersion of nanovehicles, using a FEI-Tevnai G220 S-TWIN electron microscopy with an acceleration voltage of 200 kV. The X-ray diffraction (XRD) pattern was recorded on a D/max 2500VL/PC X-ray powder diffractometer between 3° and 8° UV–vis absorption spectra were recorded from 350 nm to 800 nm using a VARIAN CARY 500 spectrophotometer in a quartz cuvette with a 1 cm light path. Fluorescence spectra were measured by a Perkin-Elmer LS-50B fluorometer with an excitation wavelength of 480 nm.

2.3. Photostability assay

To test the photostability, free HA and HANV was irradiated for a different period of time (1–5 min) using a high pressure mercury lamp with a typical power of 500 W and their UV–vis spectra was recorded every minute.

2.4. Singlet oxygen detection

The singlet oxygen generation ability of HANV and HA in aqueous solution after irradiation was evaluated using disodium salt of 9,10-anthracenedipropionic acid (ADPA) as a chemical trap (Lindig et al., 1980). ADPA can be photo-bleached by singlet oxygen to its corresponding endoperoxide and the process was monitored by recording the decrease in the absorbance of added ADPA at 379 nm (λ_{max} of ADPA) under excitation with 470 nm. Measurements were carried out according to a procedure described previously. Briefly, a 3 mL HANV or HA aqueous solution that 150 μL ADPA (5.5 mM) was placed in a quartz cuvette. The amount of m-THPC present in the NP was evaluated by its excitation and emission intensities and calculated from a calibration curve generated from free m-THPC standard solutions. The absorption intensity of ADPA when excited at 379 nm was recorded, and the solution was then irradiated using a 500 W high-voltage mercury lamp equipped with a long-pass 470 nm filter, for various time periods (i.e. 0, 30, 60, 90, 120, 150, 180 and 210 s).

2.5. HANV uptake and in vitro localization

For studying HANV's uptake and localization, the HeLa cells were trypsinized and re-suspended in medium at a concentration of 5×10^5 cells/mL, following the established protocol (Barnes and Shen, 2009). Then on 24-cell culture plates, 0.5 mL of dulbecco's modified eagle's medium (DMEM) (with 15% calf serum) was combined with 0.10 mL of cell suspension. The plates were then placed for 24 h in an incubator at 37 °C with 5% CO_2. The next day, the cells (with about 60% confluence) were changed into culture medium without calf serum but contain HANV (5 μM) and incubated at 37 °C with 5% CO_2 for 4 h. Rhodamine-123, a cationic fluorescent dye target to mitochondria, was added during the final 30 min of incubation. Then, the cells were carefully rinsed three times with phosphate-buffered saline (PBS) and then directly imaged under a fluorescence microscope.

2.6. Mitochondrial membrane potential assay

The uptake of the cationic fluorescent dye rhodamine-123 has been used for the estimation of mitochondrial membrane potential (Debbasch et al., 2001). In a typical experiment, the seeded cell in 96-well culture plates were treated with HANV (2 μM) overnight. After irradiation by different time and another 5 h incubation in dark, the cells were carefully rinsed with phosphate-buffered saline (PBS), and 100 μL of rhodamine-123 (1.0 μM) in PBS was replaced on the plates. The treated cells were returned to the incubator (37 °C, 5% CO_2) for 15 min. Next, the supernatant PBS (containing unuptaked rhodamine-123) was transfer to another new 96-well plate according to their original order. Optical density (OD) at 520 nm (λ_{max} of unuptaken rhodamine-123) was measured to evaluate mitochondrial membrane potential.

2.7. Hoechst 33342 staining

Chromatin condensation was detected by nuclear staining with Hoechst 33342 (Chen et al., 2001). After treatment with HANV overnight and irradiated by light, cells were washed with phosphate-buffered saline (PBS) three times and treated with 25 μg/mL Hoechst 33342 at 37 °C with 5% CO_2 in the dark for 15 min. Nuclear morphology change were observed under a fluorescence microscope.

2.8. Intracellular ROS detection

Intracellular ROS generation was investigated using dichlorodihydrofluorescein diacetate (DCFH-DA) assay. DCFH-DA is taken up by cells, and then activated by esterase-mediated cleavage of acetate to form dichlorodihydrofluorescein (DCFH), which is trapped in the cells. DCFH is converted to fluorescein DCF in the presence of ROS (Myhre et al., 2003). HeLa cells were seeded in 96-well plates with about 60% confluence. Following incubation with 5 μM HANV for 24 h, cells were treated with 10 μM DCFH-DA. After 15 min incubation, cells were washed twice with PBS and then exposed to light. Immediately after light exposure, cell images were acquired using an inverted fluorescence microscope. Cells that received similar treatments without HANV but exposed to light were used as controls.

2.9. Cytotoxicity studies

For studying cell viability in light-treated condition, HeLa cells at the initial concentration of 2×10^5 cells/mL were cultured on 96-cell culture plates in an incubator. After 24 h, the old medium was replaced by fresh medium (without calf serum) with HANV or HA. Cells were then incubated at 37 °C in a humidified atmosphere of 5% CO_2. Following 4 h of incubation, the culture medium was replaced by fresh medium (without calf serum) after being rinsed three times by PBS to remove adhered samples. The cells were immediately exposed to light and after 24 h incubation cell viability was estimated using 3-[4,5-dimethylthiazol-2-yl]-2,5-diphenyl tetrazolium bromide (MTT) assay (Bouquet et al., 2009).

2.10. Statistical analysis

Student's *t* test was used to analyze the differences in phototoxicity and mitochondrial membrane potential assay following treatment with free or nanovehicle-encapsulated HA. A probability level of $p < 0.05$ was considered significant (Khdair et al., 2008).

3. Result and discussion

3.1. Microscopic and spectroscopic characterizations

A typical transmission electron microscopy (TEM) image indicated that the average diameter of HANV was 110 nm and could be dispersed in the aqueous solution (Fig. 1). The final size of the silica nanovechicle is important because the lifetime of $^1O_2$ in aqueous media is in the μs regime; during which interval it can diffuse over a mean radial distances of at least 100 nm (Yan and Kopelman, 2003). X-ray powder diffraction (XRD) patterns are shown in Fig. 1. The XRD pattern displayed a characteristic diffraction peak confirmed the well-ordered mesostructure of HANV (Cheng et al., 2009).

The form of UV–vis absorption and fluorescence emission spectra of HA and HANV are similar (Fig. 2A), indicating no changes in the HA chromophore upon entrapment inside nanovehicles. The only difference is that the shape of absorption peak of 550 nm and 594 nm in HANV is not as obvious as HA. This phenomenon is caused by inhibiting intramolecular proton transfer effect of nanoparticle and silica nanovehicle (Wang et al., 2004). Silica nanovehicle entrapped HA exhibited almost the same fluorescence spectra peak with free HA at 600 nm. However, the fluorescence emission intensity of HANV was stronger than free HA (Fig. 2B) because after being embedded into nanocages, HA was protected from exposure to an aqueous environment that could cause a partial loss of fluorescence (Roy et al., 2003).

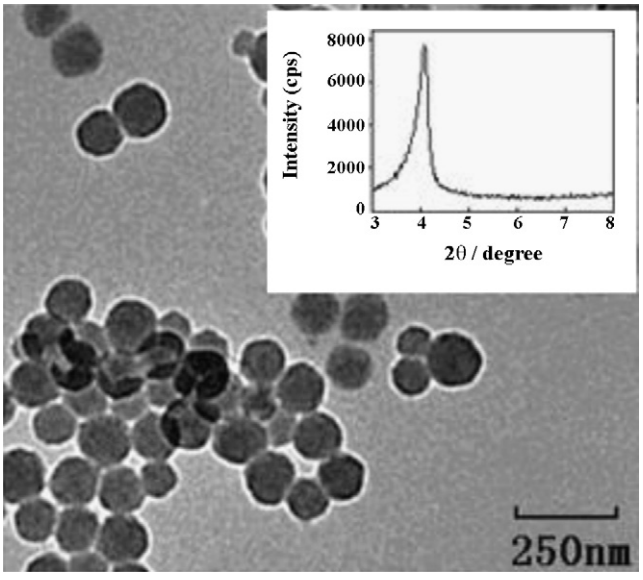

Fig. 1. TEM image of HANV. Insert panel: XRD patterns of HANV.

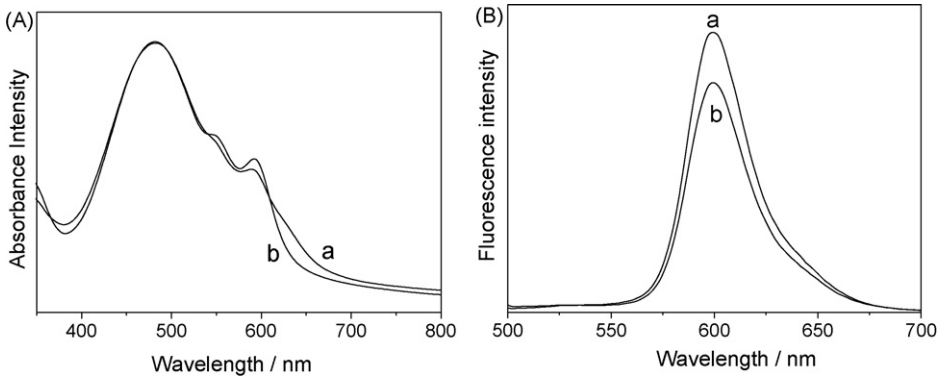

Fig. 2. (A) Ultra violet–visible (UV–visible) spectra of HANV (a) and HA (b); (B) Emission fluorescence spectra of HANV (a) and HA (b). The excitation wavelength was 480 nm.

Table 1
Photo-bleaching percentages of HANV and free HA with the prolonged irradiation time.

	1 min	2 min	3 min	4 min	5 min
HANV	2.6%	4.5%	6.0%	7.1%	9.0%
HA	5.2%	8.9%	11.1%	12.4%	14.0%

3.2. Photostability assay

The absorption intensity of HANV and HA showed the decrease at 483 nm as a function of the irradiation time, which illustrated the photo-bleaching of HA. Under the same experimental conditions, photo-bleached percent of HANV and free HA are 9.02% and 14.04%, respectively (Table 1). The result indicated that after encapsulation, most photosensitizers could maintain their integrity under laser irradiation as compared to the case of free HA (Cheng et al., 2009). The protection by silica nanovehicle offers better photostability of HA against bleaching. The increased fluorescence intensity and lessened photo-bleaching effect of entrapped HA in aqueous media is very desirable in bioimaging applications.

3.3. Singlet oxygen generation

Singlet oxygen can be detected using a chemical method by the photo-oxidation of the disodium salt of 9,10-anthracenedipropionic acid (ADPA) to its endoperoxide derivative. Equimolar solutions of ADPA containing HANV or free HA were irradiated. In the presence of HANV, the anthracene absorbance intensity showed a continuous sharp decrease over 210 s (Fig. 3A). In contrast, only minimal photo-bleaching of ADPA was observed under the same experiment condition in the control experiments when free HA was used as the sensitizer. This confirms that the presence of the silica nanovehicle significantly increases the ability of HA to generate singlet oxygen because the nanovehicle protected and retained the long-lived singlet state of HA (Mahmoudi et al., 2009).

According to the tailored specifically equations reported by Raoul Kopelman's group (Yan and Kopelman, 2003; Tang et al., 2005), the exact reaction rate constant (k) with ADPA for HANV and free HA is shown to be 3.3×10^{-3}/s (correlation coefficient $R = 0.99917$) and 1.5×10^{-3}/s ($R = 0.99955$), respectively (Fig. 3B). And singlet oxygen quantum yield (Φ_Δ) of HANV was calculated on the basis of Eqs. (1) and (2).

$$\Phi_\Delta^S = \Phi_\Delta^R \frac{k^S I_{aT}^R}{k^R I_{aT}^S} \quad (1)$$

$$I_a = I_0(1 - e^{-2.3A}) \quad (2)$$

here, superscript S and R indicate the sample and reference compound, respectively. I_a is the total amount of light absorbed by the sensitizers. A is the corresponding absorbance at irradiation wavelength (Chen et al., 2008; Musil et al., 2007). The calculation results showed that the $^1O_2$ quantum yield is 2.13 (taking free HA as a reference and defining its $^1O_2$ quantum yield is 1 at this experiment condition), which suggest that the singlet oxygen production from HA embedded in silica nanovehicle exceeds that of free HA.

3.4. Uptake and intracellular distribution of HANV

Fluorescence microimaging was used to determine whether HANV was taken up by tumor cells. The fluorescence images of HeLa cells demonstrated the active uptake of drug-doped nanovehicle into the tumor cells. The cells were viable (verified morpholog-

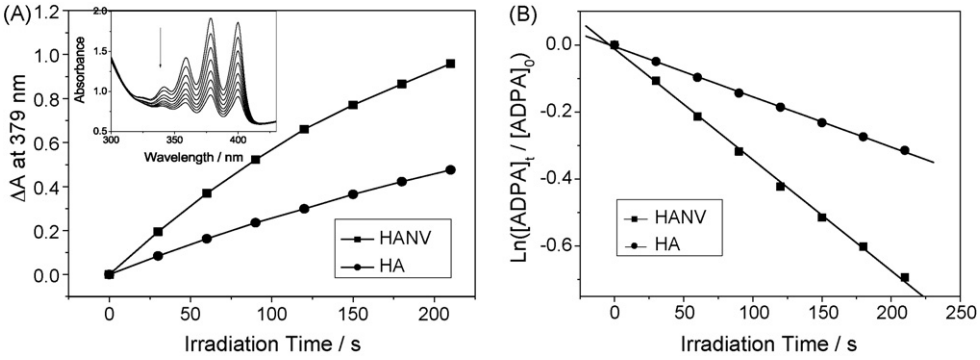

Fig. 3. (A) Photosensitized ADPA bleaching by measuring absorbance decrease (ΔA) at 379 nm (λ_{max} of ADPA) as a function of irradiation time. Insert panel: Photo-bleaching of ADPA by singlet oxygen generated by HANV after irradiation with light for 0, 30, 60, 90, 120, 150, 180 and 210 s. (B) The best fit of the reaction rate constant with ADPA by HANV and free HA.

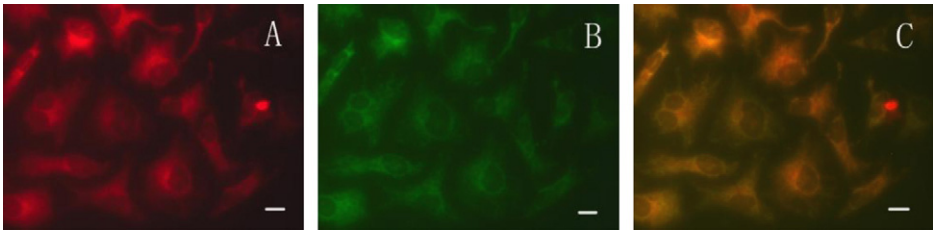

Fig. 4. Dual fluorescence labeling for HANV (a) red fluorescence and rhodamine-123 (b) green fluorescence in control HeLa cells. The merged image (c) demonstrates that the two fluorescence signals co-locate in mitochondria. Bar = 20 nm (For interpretation of the references to color in this figure legend, the reader is referred to the web version of the article).

ically) in the dark even after 24 h of staining, indicating low dark toxicity from the vehicles. Furthermore, we checked the subcellular localization of HANV in HeLa cells by fluorescence microscopy. As a lipophilic cation and an efficient mitochondrial probe, rhodamine-123 should localize to mitochondria. Indeed, when the cells were incubated with HANV together with rhodamine-123, the fluorescence pattern of HANV coincided with that of the mitochondrial probe (Fig. 4). The results indicated that the HANV localize in the same subcellular region as the mitochondrial marker, suggesting its affinity to mitochondria.

3.5. *Effects of HANV on* $\Delta\Psi_m$

Further evidence for the mitochondria localization of HANV was mitochondrial membrane potential ($\Delta\Psi_m$) change after uptake HANV and irradiated by light. Rhodamine-123 is widely used to make dynamic measurements of mitochondrial membrane potential both *in vitro* and in situ because $\Delta\Psi_m$ is proportional to unuptaked rhodamine-123 (Cao et al., 2007) and $\Delta\Psi_m$ change always associate with the cell apoptosis (Wang et al., 2009). After exposure to light for 1–3 min, there was a dose-dependent increase in $\Delta\Psi_m$ (Fig. 5), indicating that mitochondria were hyperpolarized. However, a decline in the $\Delta\Psi_m$ was detected after irradiated longer than 3 min (4–5 min). Our data indicate that exposure to light results in a biphasic change in $\Delta\Psi_m$ with an early hyperpolarization (1–3 min), followed by a later depolarization and $\Delta\Psi_m$ collapse (4–5 min) and the $\Delta\Psi_m$ change degree of the HANV treated cell was intenser than HA and control one.

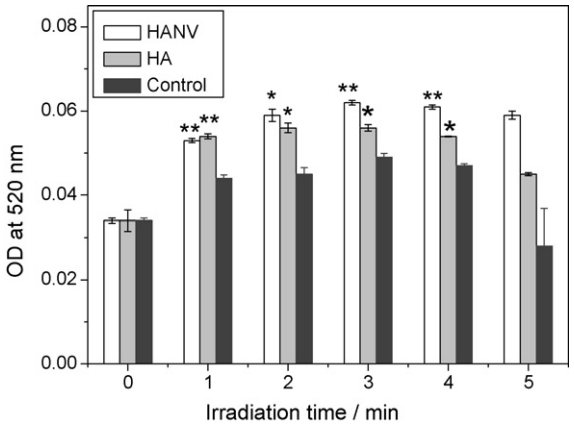

Fig. 5. Effect of HANV and HA on mitochondrial membrane potential. (*$p < 0.05$ vs. Control, **$p < 0.01$ vs. Control; Control: cells were exposed to light without HANV or HA).

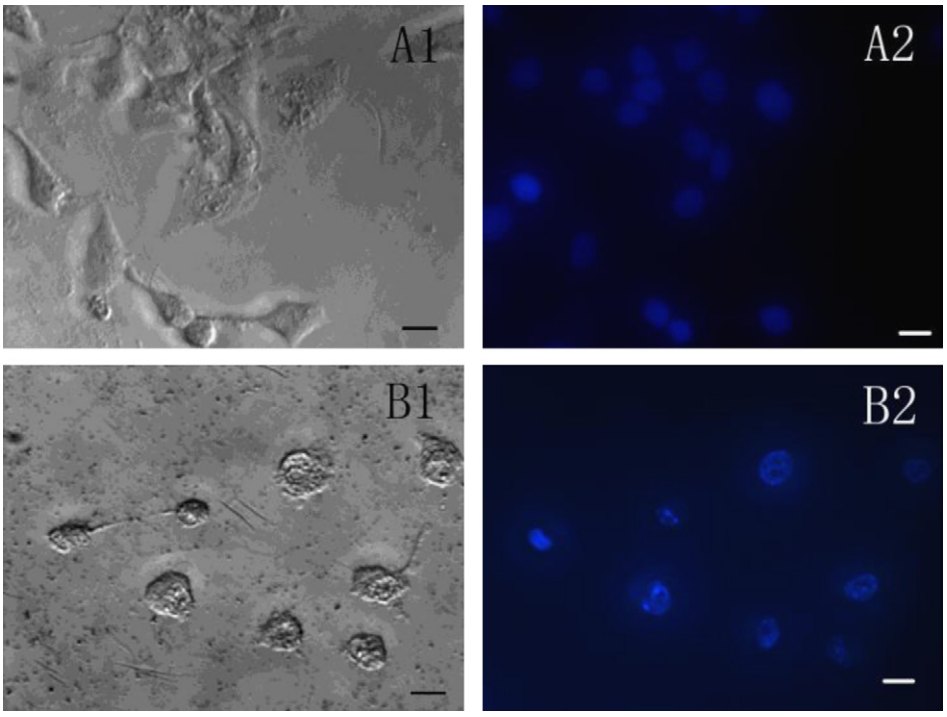

Fig. 6. Morphology of HeLa cells and Hoechst 33342 staining of HeLa cells incubated with HANV for 24 h in the dark (A) or with light irradiation (B). Bar = 20 nm.

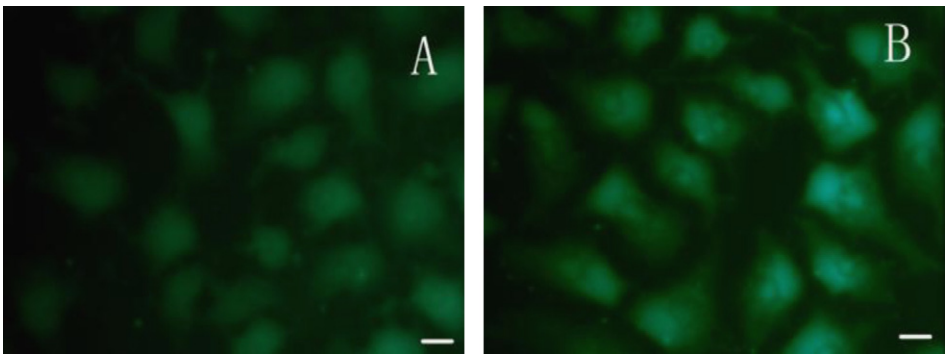

Fig. 7. ROS in HeLa cells treated without and with HANV after irradiation by detecting the DCF fluorescence. Bar = 20 nm.

3.6. Effects of HANV on apoptosis induction

The Hoechst 33342 staining is sensitive to DNA and was used to assess changes in nuclear morphology. PDT process will damage DNA in nuclear of cancer calls by activating PSs by light, so DNA damage is a very important index in PDT. The results showed that there is no significant change in cell morphology (Fig. 6A1) when the cells treated with HANV but without irradiation and the fluorescence of chromatin stained dimly and occupied the majority of the cell (Fig. 6A2), indicating low dark toxicity from the vehicles. In contrast, the cells shrinked after treating with HANV and irradiation by light (Fig. 6B1); at the same time, apoptotic features such as nuclear shrinkage, chromatin condensation or fragmentation were demonstrated and the fluorescence of chromatin was condensed, intensely stained, or shifted to the periphery of the cell (Fig. 6B2).

3.7. Intracellular ROS generation

To monitor ROS generation caused by HANV *in vitro*, the fluorescent products DCF were determined by fluorescence microscopy. HeLa cells were labeled with DCFH-DA for 30 min and imaged after irradiation. Non-HANV treated cells under the same experimental procedures were used as control and the fluorescence detected in these cells was weak and spread all over the cells. An increased fluorescence was detected in the cells treated with HANV (Fig. 7A) and these cells exhibit stronger fluorescence intensity in cytoplasm, where is the place that HANV accumulated, indicating the intracellular ROS generation mediated by HANV (Fig. 7B), which imply that HANV is promising candidate with high light-toxicity to cancer cells *in vitro*.

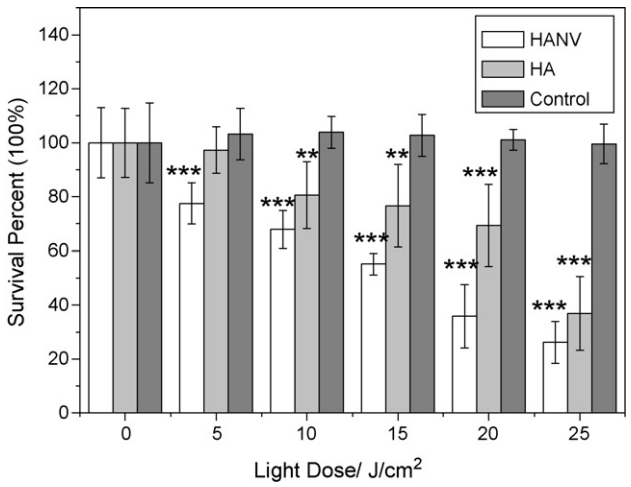

Fig. 8. Light dose response demonstrating enhanced cytotoxicity following PDT with HANV (2 μM) comparing with free HA (2 μM). (**$p < 0.01$ vs. Control, ***$p < 0.001$ vs. Control; Control: cells were exposed to light without HANV or HA).

3.8. Photodynamic effects in vitro

Phototoxicity of HANV and HA was estimated by means of the colorimetric MTT assay. The ranges of HANV and free HA concentrations required to exert 50% toxicity (IC_{50}) under irradiation can be estimated from the cell survival rate. When the light dose was 5 J/cm^2, the IC_{50} of HANV and free HA was 0.45 μg/mL (the concentration of HA in nanovehicles) and 0.56 μg/mL, separately.

In addition, various doses of light have been used in this study, and it was found, following MTT assays, that the cell viability has a sharp decrease as the light dose increases and the photodamage degree of HANV was higher than free HA (Fig. 8). The data show that HANV is an effective drug deliver system for killing tumor cells *in vitro* by light exposure.

4. Conclusion

In this paper, we have described a preparation and characterization of a silica nanovehicle using a new sol–gel method and studied its application in photodynamic therapy *in vitro*. Two steps were contained in this procedure: (I) hydrophobic photosensitizer nanoparticle was prepared by "reprecipitation method" in water and (II) HA nanoparticle was surrounded by AETPS molecules through intermolecular hydrogen bonding between the hydroxyl groups of PS molecules and the amine moieties of AETPS and AETPS molecules were hydrolyzed and polymerized in situ to encapsulate the PS nanoparticle in situ. Comparing with traditional methods, this preparation procedure was simple but effective. Besides, no more additional catalysts or surfactants were used during the preparation procedure, which can greatly simplify the reaction system. Based on the conception, hypocrellin A was encapsulated in silica nanovehicle using this method and the efficacy of encapsulation and the potential application in photodynamic therapy were verified.

The results show that about 110 nm silica nanovehicle, with good dispersibility and well-ordered mesostructure, was prepared by this method and encapsulation efficacy was satisfied. The photostability result indicated that after encapsulation most photosensitizers could maintain their integrity under laser irradiation as compared to the case of free HA caused by the protection by silica nanovehicle. *In vitro* experiments illustrated that HANV was actively taken up by HeLa cells, localized in mitochondria and finally destroyed the mitochondria membrane after irradiation. Moreover, the singlet generation ability was also great improved, which was verified by its superior cancer cell damage ability comparing with free HA. All these results showed that this method

was feasible and have great application potential in drug delivery system.

Acknowledgment

This research was supported by the National Natural Science Foundation of China (No. 20603018) and the Key Laboratory of Photochemical Conversion and Optoelectronic Materials, TIPC, CAS.

References

An, B.K., Kwon, S.K., Jung, S.D., Park, S.Y., 2002. Enhanced emission and its switching in fluorescent organic nanoparticles. J. Am. Chem. Soc. 124, 14410–14415.

Baba, K., Pudavar, H.E., Roy, I., Ohulchanskyy, T.Y., Chen, Y.H., Pandey, R.K., Prasad, P.N., 2007. New method for delivering a hydrophobic drug for photodynamic therapy using pure nanocrystal form of the drug. Mol. Pharm. 4, 289–297.

Barnes, M.P., Shen, W.C., 2009. Disulfide and thioether linked cytochrome *c*-oligoarginine conjugates in HeLa cells. Int. J. Pharm. 369, 79–84.

Bouquet, W., Boterberg, T., Ceelen, W., Pattyn, P., Peeters, M., Bracke, M., Remon, J.P., Vervaet, C., 2009. *In vitro* cytotoxicity of paclitaxel/β-cyclodextrin complexes for HIPEC. Int. J. Pharm. 367, 148–154.

Cao, J., Liu, Y., Jia, L., Zhou, H.M., Kong, Y., Yang, G., Jiang, L.P., Li, Q.J., Zhong, L.F., 2007. Curcurnin induces apoptosis through mitochondrial hyperpolarization and mtDNA damage in human hepatoma G_2 cells. Free Radical Biol. Med. 43, 968–975.

Chen, C.T., Burton-Wurster, N., Borden, C., Hueffer, K., Bloom, S.E., Lust, G., 2001. Chondrocyte necrosis and apoptosis in impact damaged articular cartilage. J. Orthop. Res. 19, 703–711.

Cheng, S.H., Lee, C.H., Yang, C.S., Tseng, F.G., Mou, C.Y., Lo, L.W., 2009. Mesoporous silica nanoparticles functionalized with an oxygen-sensing probe for cell photodynamic therapy: potential cancer theranostics. J. Mater. Chem. 19, 1252–1257.

Cheng, Y., Samia, A.C., Meyers, J.D., Panagopoulos, I., Fei, B.W., Burda, C., 2008. Highly efficient drug delivery with gold nanoparticle vectors for *in vivo* photodynamic therapy of cancer. J. Am. Chem. Soc. 130, 10643–10647.

Corr, S.A., Gun'ko, Y.K., Douvalis, A.P., Venkatesan, M., Gunning, R.D., Nellist, P.D., 2008. From nanocrystals to nanorods: New iron oxide-silica nanocomposites from metallorganic precursors. J. Phys. Chem. C. 112, 1008–1018.

Debbasch, C., Brignole, F., Pisella, P.J., Warnet, J.M., Rat, P., Baudouin, C., 2001. Quaternary ammoniums and other preservatives' contribution in oxidative stress and apoptosis on Chang conjunctival cells. Investigative Ophthalmol. Visual Sci. 42, 642–652.

Ferrer, M.L., Yuste, L., Rojo, F., del Monte, F., 2003. Biocompatible sol-gel route for encapsulation of living bacteria in organically modified silica matrixes. Chem. Mater. 15, 3614–3618.

Frenkel-Mullerad, H., Avnir, D., 2005. Sol-gel materials as efficient enzyme protectors: preserving the activity of phosphatases under extreme pH conditions. J. Am. Chem. Soc. 127, 8077–8081.

Fu, H.B., Yao, J.N., 2001. Size effects on the optical properties of organic nanoparticles. J. Am. Chem. Soc. 123, 1434–1439.

Hulchanskyy, T.Y., Roy, I., Goswami, L.N., Chen, Y., Bergey, E.J., Pandey, R.K., Oseroff, A.R., Prasad, P.N., 2007. Organically modified silica nanoparticles with covalently incorporated photosensitizer for photodynamic therapy of cancer. Nano Lett. 7, 2835–2842.

Kim, S., Ohulchanskyy, T.Y., Pudavar, H.E., Pandey, R.K., Prasad, P.N., 2007. Organically modified silica nanoparticles co-encapsulating photosensitizing drug and aggregation-enhanced two-photon absorbing fluorescent dye aggregates for two-photon photodynamic therapy. J. Am. Chem. Soc. 129, 2669–2675.

Kim, S., Ohulchanskyy, T.Y., Bharali, D., Chen, Y., Pandey, R.K., Prasad, P.N., 2009. Organically modified silica nanoparticles with intraparticle heavy-atom effect on the encapsulated photosensitizer for enhanced efficacy of photodynamic therapy. J. Phys. Chem. C. 113, 12641–12644.

Khdair, A., Gerard, B., Handa, H., Mao, G.Z., Shekhar, M.P.V., Panyam, J., 2008. Surfactant-polymer nanoparticles enhance the effectiveness of anticancer photodynamic therapy. Mol. Pharm. 5, 795–807.

Lindig, B.A., Rodgers, M.A.J., Schaap, A.P., 1980. Determination of the lifetime of singlet oxygen in D2O using 9,10-anthracenedipropionic acid, a water-soluble probe. J. Am. Chem. Soc. 102, 5590–5593.

Mahmoudi, M., Simchi, A., Imani, M., Milani, A.S., Stroeve, P., 2009. An in vitro study of bare and poly (ethylene glycol)-co-fumarate-coated superparamagnetic iron oxide nanoparticles: a new toxicity identification procedure. Nanotechnology 20, 225104.

Musil, Z., Zimcik, P., Miletin, M., Kopecky, K., Petrik, P., Lenco, J., 2007. Influence of electron-withdrawing and electron-donating substituents on photophysical properties of azaphthalocyanines. J. Photochem. Photobiol. A. 186, 316–322.

Myhre, O., Andersen, J.M., Aarnes, H., Fonnum, F., 2003. Evaluation of the probes 2',7'-dichlorofluorescin diacetate, luminol, and lucigenin as indicators of reactive species formation. Biochem. Pharmacol. 65, 1575–1582.

Piao, Y., Burns, A., Kim, J., Wiesner, U., Hyeon, T., 2008. Designed fabrication of silica-based nanostructured particle systems for nanomedicine applications. Adv. Funct. Mater. 18, 3745–3758.

Roy, I., Ohulchanskyy, T.Y., Pudavar, H.E., Bergey, E.J., Oseroff, A.R., Morgan, J., Dougherty, T.J., Prasad, P.N., 2003. Ceramic-based nanoparticles entrapping water-insoluble photosensitizing anticancer drugs: a novel drug carrier system for photodynamic therapy. J. Am. Chem. Soc. 125, 7860–7865.

Sadzuka, Y., Iwasaki, F., Sugiyama, I., Horiuchi, K., Hirano, T., Ozawa, H., Kanayama, N., Sonobe, T., 2007. Study on liposomalization of zinc-coproporphyrin I as a novel drug in photodynamic therapy. Int. J. Pharm. 338, 306–309.

Tang, W., Xu, H., Kopelman, R., Philbert, M.A., 2005. Photodynamic characterization and *in vitro* application of methylene blue-containing nanoparticle platforms. Photochem. Photobiol. 81, 242–249.

Tu, H.L., Lin, Y.S., Lin, H.Y., Hung, Y., Lo, L.W., Chen, Y.F., Mou, C.Y., 2009. *In vitro* studies of functionalized mesoporous silica nanoparticles for photodynamic therapy. Adv. Mater. 21, 172–177.

Wang, S.Z., Gao, R.M., Zhou, F.M., Selke, M.J., 2004. Nanomaterials and singlet oxygen photosensitizers: potential applications in photodynamic therapy. J. Mater. Chem. 14, 487–493.

Wang, W., Xiong, W., Wan, J.L., Sun, X.H., Xu, H.B., Yang, X.L., 2009. The decrease of PAMAM dendrimer-induced cytotoxicity by PEGylation via attenuation of oxidative stress. Nanotechnology 20, 105103.

Xiao, D.B., Lu, X., Yang, W.S., Fu, H.B., Shuai, Z.G., Fang, Y., Yao, J.N., 2003. Size-tunable emission from 1,3-diphenyl-5-(2-anthryl)-2-pyrazoline nanoparticles. J. Am. Chem. Soc. 125, 6740–6745.

Yan, F., Kopelman, R., 2003. The embedding of meta-tetra(hydroxyphenyl)-chlorin into silica nanoparticle platforms for photodynamic therapy and their singlet oxygen production and pH-dependent optical properties. Photochem. Photobiol. 78, 587–591.

Zhou, J.H., Zhou, L., Dong, C., Feng, Y.Y., Wei, S.H., Shen, J., Wang, X.S., 2008. Preparation and photodynamic properties of water-soluble hypocrellin A-silica nanospheres. Mater. Lett. 62, 2910–2913.

Zhou, L., Dong, C., Wei, S.H., Feng, Y.Y., Zhou, J.H., Liu, J.H., 2009a. Water-soluble soft nano-colloid for drug delivery. Mater. Lett. 63, 1683–1685.

Zhou, L., Zhou, J.H., Dong, C., Ma, F., Wei, S.H., Shen, J., 2009b. Water-soluble hypocrellin A nanoparticles as a photodynamic therapy delivery system. Dyes Pigments 82, 90–94.